Sains Malaysiana 52(3)(2023): 953-966
http://doi.org/10.17576/jsm-2023-5203-19

Green Synthesis of Silver Nanoparticle Decorated on Reduced Graphene Oxide Nanocomposite using *Clinacanthus nutans* and Its Applications

(Sintesis Hijau Nanozarah Perak Dihiasi pada Nanokomposit Grafin Oksida Terturun menggunakan *Clinacanthus nutans* dan Penggunaannya)

Dharshini Perumal[1], Che Azurahanim Che Abdullah[1,2,3*], Emmellie Laura Albert[3] & Ruzniza Mohd Zawawi[4]

[1]Biophysics Laboratory, Department of Physics, Faculty of Science, Universiti Putra Malaysia, 43400 UPM Serdang, Selangor Darul Ehsan, Malaysia
[2]UPM-MAKNA Cancer Research Laboratory, Institute of Bioscience, Universiti Putra Malaysia, 43400 UPM Serdang, Selangor Darul Ehsan, Malaysia
[3]Institute of Nanoscience and Nanotechnology, Universiti Putra Malaysia, 43400 UPM Serdang, Selangor Darul Ehsan, Malaysia
[4]Department of Chemistry, Faculty of Science, Universiti Putra Malaysia, 43400 UPM Serdang, Selangor Darul Ehsan, Malaysia

Received: 20 September 2022/Accepted: 4 January 2023

ABSTRACT

A straightforward approach that uses *Clinacanthus nutans* leaf extract as a bio-reduction agent has been reported to anchor silver nanoparticles onto graphene oxide (rGO-Ag). The nanocomposite was characterized by using ultraviolet-visible spectroscopy, Fourier transform infrared spectroscopy, field emission scanning electron microscopy with energy-dispersive X-ray spectroscopy, and X-ray diffraction. A qualitative colour transition from yellowish to dark brown confirmed the biosynthesis of rGO-Ag nanocomposite and showed a surface plasmon resonance at 263 nm and 425 nm. Utilizing cyclic voltammetry, the electrochemical characteristics of the rGO-Ag nanocomposite modified screen printed carbon electrodes were examined. The rGO-Ag nanocomposite electrode enhanced anodic current approximately 1.29 times greater compared to silver nanoparticles (AgNPs) and 1.34 times greater compared to graphene oxide (GO). Moreover, rGO-Ag nanocomposites exhibited excellent antibacterial activity against typical Gram-positive (*S. aureus*) (11.99 ± 0.26 mm) and Gram-negative (*E. coli*) (11.86 ± 0.29 mm) bacteria. Toxicity was assayed using brine shrimp *Artemia salina*. The results of hatching and mortality assay demonstrates that AgNPs and rGO-Ag nanocomposite is biocompatible with *A. salina* at a low dosage (0.001 mg/mL). This work offers a guide for the future synthesis of nanocomposites using green reductants. The as- synthesized nanocomposite shows a promising component for the development of biomedical devices applications.

Keywords: Electrochemical; green synthesis; reduced graphene oxide; silver nanoparticles; toxicity

ABSTRAK

Pendekatan ringkas menggunakan ekstrak daun *Clinacanthus nutans* sebagai agen bio-penurunan telah dilaporkan berjaya melekatkan nanozarah perak pada grafin oksida (rGO-Ag). Spektroskopi ultralembayung, spektroskopi inframerah transformasi Fourier, mikroskop elektron pengimbasan pelepasan medan dengan spektroskopi penyebaran tenaga sinar-X dan spektroskopi pembelauan sinar-X digunakan untuk menghuraikan ciri nanokomposit yang terbentuk. Peralihan warna secara kualitatif daripada kekuningan kepada coklat gelap mengesahkan keberhasilan biosintesis nanokomposit rGO-Ag selain kewujudan resonans plasmon permukaan pada 263 nm dan 425 nm. Dengan menggunakan kitaran voltammetri, ciri elektrokimia bagi skrin bercetak elektrod karbon diubah suai dengan rGO-Ag nanokomposit telah diperiksa. Keputusan menunjukkan bagi nanokomposit rGO-Ag peningkatan arus anod adalah kira-kira 1.29 kali lebih besar berbanding dengan nanozarah perak (AgNPs) dan 1.34 kali lebih besar berbanding dengan grafin oksida (GO). Selain itu, nanokomposit rGO-Ag menunjukkan aktiviti antibakteria yang sangat baik terhadap

bakteria Gram-positif (*S. aureus*) (11.99 ± 0.26 mm) dan Gram-negatif (*E. coli*) (11.86 ± 0.29 mm). Ketoksikan telah diuji menggunakan udang air garam *Artemia salina*. Keputusan penetasan dan asai kemortalan menunjukkan bahawa AgNPs dan rGO-Ag nanokomposit adalah bioserasi dengan *A. salina* pada dos yang rendah (0.001 mg/mL). Kajian ini memberikan panduan dalam sintesis nanokomposit menggunakan kaedah penurunan hijau pada masa akan datang. Nanokomposit yang telah disintesis menunjukkan potensi untuk diguna pakai sebagai komponen dalam bidang aplikasi peranti bioperubatan.

Kata kunci: Elektrokimia; grafin oksida terturun; ketoksikan; nanozarah perak; sintesis hijau

Introduction

Graphene, a single layer of graphite that has undergone sp^2 hybridization, is arranged in a two-dimensional enclosed hexagonal honeycomb lattice (Handayani et al. 2022). Graphene has long been regarded as a desirable material because of its large 2D surface area and superior thermal, physical, chemical, and mechanical characteristics (Dominic et al. 2022). Due to its excellent qualities, graphene can be employed in a wide range of applications, such as hydrogen production, energy storage, solar cells, super capacitors, electronic devices, and biosensors (Olorunkosebi et al. 2021; Parthipan et al. 2021).

Recent graphene nanotechnology advancements have focused primarily on integrating it with other organic and inorganic materials to provide varied and useful features. Due to the peculiar electron distribution between the carbon and metal in metal nanoparticles, their integration with graphene has enormous potential (Abboud et al. 2016). The most practical and affordable method of producing graphene flakes is through chemical exfoliation. However, this process frequently yields graphene oxide (GO) rather than pure graphene. Therefore, the generated GO must be reduced, with the functional groups on the GO being eliminated and its conductivity being returned to the same level as that of graphene, to fulfill the requirements of high-performance devices (Bal, Tumer & Kose 2022). Reduced graphene oxide (rGO) is created during the reduction procedure, which involves removing oxygen functional groups from the edges and basal plane of the GO (Rai et al. 2021). Due to their superior electrochemical reduction, researchers have demonstrated that placing metal nanoparticles on rGO brings about greater advantages in sensing applications than other support materials (Bhangoji et al. 2021).

Due to their versatile features, nanoparticles of metals like gold, zinc, copper, magnesium, platinum, palladium, and silver have attracted considerable attention and have been used in various applications (Allafchian et al. 2022; Mahendran et al. 2021). Of these metal nanoparticles, silver nanoparticles (AgNPs) are particularly well-known and have been used more frequently in various fields due to their optical, catalytic, and electrical qualities. Numerous biological capabilities of AgNPs have been reported, including in anti-inflammatory, antimicrobial, antifungal, anticancer, and cancer cell destruction applications (Herbin et al. 2022; Rudrappa et al. 2022). AgNPs on reduced graphene oxide (rGO-AgNPs) have recently been demonstrated to offer more electrochemically active surface areas, effectively accelerating the electron transfer between the electrode and detecting molecules, which results in a quick and sensitive current response (Pumera 2010). rGO-AgNPs composites can be employed to sense substances including glucose (Tran et al. 2020), ammonia (Jarmoshti et al. 2019), chromium (VI) ions, carbaryl pesticide (Minh et al. 2020), and 4-nitrophenol (Ahmad et al. 2020)an electrochemical sensor for the detection of 4-Nitrophenol (referred to as 4-NP.

The fabrication of metal nanoparticle-rGO composites, however, still faces several obstacles. In terms of the synthesis, several physical and chemical processes have been extensively studied. These procedures, however, must overcome obstacles like complex experimental setups or hazardous chemical reagents in the form of reducing, capping, or stabilizing agents. For instance, most synthetic procedures require dangerous reducing agents including metal hydrides, sodium borohydride, hydroquinone, dimethyl-hydrazine, and hydrazine (Mindivan & Göktaş 2020). The efficacy of metal nanoparticle-rGO composites is also reduced with the use of surfactants or expensive stabilizing agent molecules, which are added to and firmly absorbed onto the metal nanoparticle surfaces (Dinh et al. 2014).

Phytoconstituents are excellent substitutes for traditional hazardous compounds due to their non-toxic and environmentally benign character (Yang et al. 2021).

Because of their low toxicity, affordability, and ease of use compared to synthetic drugs, plant extracts from traditional medicinal plants are widely used in Southeast Asian countries. These extracts are renowned for their medicinal properties, which include antimicrobial, antioxidant, anticancer, anti-inflammatory, and anti-diabetic properties that aid in the recovery from diseases and promote overall health. In products made from medicinal plants, numerous bioactive substances can be identified (Chinnaraj et al. 2021).

The Acanthaceae family includes *Clinacanthus nutans*, sometimes referred to as 'belalai gajah' in Malaysia (Ooi et al. 2021). The members of this family are rich in flavonoids, phenolics, steroids, triterpenoids, cerebrosides, glycoglycerolipids, glycerides, and sulfur-containing glycosides, making them a fascinating element of a nutritious diet and effective folk remedies (Yu et al. 2022). Diabetes, cancer, herpes infections, inflammation, and various skin conditions have all been traditionally treated with this plant. Numerous pharmacological activities of *C. nutans* have been documented, including anti-inflammatory, antiviral, antioxidant, antibacterial, antidiabetic, antihyperlipidemic, and anticancer actions (Azemi, Mokhtar & Rasool 2020).

This study suggests that *C. nutans* leaf extract can be used as a nontoxic reducing agent to prepare AgNPs and reduced graphene oxide decorated silver (rGO-Ag) nanocomposites in a quick, simple, low-cost, and environmentally friendly manner. Different microscopic, spectroscopic, and analytical methods were used to analyze the as-synthesized nanocomposites, including ultraviolet-visible spectroscopy (UV-vis), field emission scanning electron microscopy (FESEM), X-ray energy dispersive spectroscopy (EDS), X-ray diffraction (XRD), and Fourier transform infrared spectroscopy (FTIR). Very few studies have reported the environmental toxicity of the as-synthesized nanocomposite. Hence, we have conducted the toxicity using a zooplankton called *Artemia salina*. The antimicrobial and electrochemical sensing capabilities of the nanocomposites were also investigated. The findings support the development of green rGO-Ag nanocomposite for use in development of biomedical devices applications.

Materials and Methods

Graphite powder, <20 μm was purchased from Sigma Aldrich. Silver nitrate ($AgNO_3$) was purchased from ChemiZ (M) Sdn. Bhd., Malaysia. Sulfuric acid (H_2SO_4, 98%), phosphoric acid (H_3PO_4, 85%), hydrogen peroxide (H_2O_2, 30%), hydrochloric acid (HCl, 37%), ethyl alcohol, and potassium permanganate ($KMnO_4$) powder were obtained from R&M chemicals. Potassium Hexacyanoferrate (III) was bought from Friedemann Schmidt. Potassium chloride (KCl) was bought from Chemiz (M) Sdn. Bhd., Malaysia. Screen-printed carbon electrodes (Dropsens C110) with a 4 mm diameter were purchased from Metrohm Malaysia Sdn. Bhd. Milli-Q (18.2 MΩ-cm) was utilized for this study.

Graphene oxide preparation

Graphene oxide (GO) was synthesized from graphite powder using the Improved Hummer procedure (Marcano et al. 2010).

Silver nanoparticle synthesis

Preparation of the *C. nutans* leaf extract: The leaves were thoroughly washed with water and oven-dried. The dried *C. nutans* leaves were pulverized and finely ground. For this experiment, 15 g of finely powdered leaves was added to 150 mL of DI water in a 500 mL round-bottomed flask. The mixture was then refluxed for 30 min at 90 °C in an oil bath to extract the compounds from the leaves into the water. The mixture was centrifuged for 10 min at 3,500 rpm to remove bulk trash after it had been cooled to room temperature. Lastly, to remove any remaining trace particles, the resulting supernatant was filtered through Whatman filter paper. The filtrate containing the *C. nutans* leaf extract was stored in a refrigerator (4 °C) for future use.

AgNPs synthesis using a green method: A conventional procedure was used to create the 0.1 M silver nitrate ($AgNO_3$) aqueous solution. First, 50 mL of $AgNO_3$ solution was added to a 250 mL round-bottomed flask for reduction into Ag^+ ions, with silver foil used to shield the solution from light. Then, 50 mL of freshly made *C. nutans* leaf extract was added drop by drop to the $AgNO_3$ solution while it was being continuously stirred. To prevent the photoactivation of the delicate $AgNO_3$, the mixture was kept in the dark at a reflux setting of 100 °C for 6 h while being stirred. At first, the mixture seemed to be light yellow but it quickly turned dark brown, indicating the creation of AgNPs. The dark brown mixture was centrifuged at 3,500 rpm for 15 min. Purified nanoparticles were obtained by periodically washing the precipitate with water. After being freeze-dried, the AgNPs produced were used for characterization to establish the nature of the nanoparticles.

Preparation of the rGO-Ag nanocomposites

The rGO-Ag nanocomposites were prepared using a one-pot reaction. Briefly, 50 mg of GO was dispersed in 50 mL of water and sonicated for 1 h. A 250 mL round-bottomed flask containing a GO suspension was supplemented with 50 mL of 0.1 M aqueous solution of $AgNO_3$. The combined mixture was then stirred continuously as 50 mL of aqueous *C. nutans* leaf extract was added dropwise and heated at 100 °C in a reflux setting for 6 h. After the reaction had finished, the resulting rGO-Ag nanocomposites were centrifuged, repeatedly rinsed with water, and freeze-dried.

Characterization

The size, shape, and functional groups of the as-synthesized AgNPs and rGO-AgNPs nanocomposites were determined using the approaches described as follows. The plasmonic peaks of the as-prepared sample were noticed to range between 200 and 700 nm using UV-visible spectrophotometry (Jenway 7315, Staffordshire, UK). The crystalline structure of the as-synthesized sample was investigated using an X-ray diffractometer (SmartLab, Rigaku, Tokyo, Japan). The FT-IR spectra of the as-prepared sample were captured in the 400–4000 cm^{-1} range using an FTIR spectrometer (FTIR-spectrum 400, Perkin Elmer, USA). A scanning electron microscope (Clara, Tescan) was used to examine the prepared sample inbuild with an energy-dispersive X-ray spectrometer (EDS).

Antibacterial activity studies

Using the disc diffusion method, the antibacterial activity of the GO, AgNPs, and rGO-Ag nanocomposites was assessed against the Gram-negative bacteria *Escherichia coli* (ATCC 25922) and the Gram-positive bacterium *Staphylococcus aureus* (ATCC 43300). A triplicate agar medium plate was used for the analysis after the disc (size 6 mm) containing 20 µL of the as-prepared sample (1 mg/mL) had been placed on test plates with streaking bacteria. A millimeter ruler was used to assess the zone of inhibition following a 24 h incubation period at 37 °C.

Preparation of rGO-Ag nanocomposite-modified screen-printed carbon electrodes (SPCEs)

The electrochemical measurements of the rGO-Ag nanocomposite were carried out utilizing the Metrohm Multi Autolab M101 and Nova 2.1.4 software (Barendrecht, Netherlands). The rGO-Ag nanocomposite was deposited onto SPCEs by drop-casting the solution, after which it was dried under a nitrogen stream. The rGO-Ag-SPCE was used immediately for analysis. At a scan rate of 100 mV/s, cyclic voltammetry was carried out at a range of -0.3 V to 0.7 V.

Hatching percentage of Artemia Cyst

A 96-well plate was used for the experiment. The desired concentration of the as-synthesized material (0, 0.001, 0.01, 0.1, 1.0 mg/mL) was added to each well, which contained 10 *Artemia salina* cysts. Five duplicates of each test concentration were performed. To create a conducive environment for the cysts to hatch, the experimental setup was exposed to light. After 24, 48, and 72 h of incubation, the number of hatched cysts was determined. For various test concentrations, the hatching percentage was calculated. The outcomes were tabulated, and a graph was created.

Mortality percentage of Artemia nauplii

A mortality test was performed on five replicates of nauplii collected 24 h after hatching, which corresponded approximately to first instar (stage I). Each well of the 96-well plate containing the as-synthesized sample material at the specified concentrations (0, 0.001, 0.01, 0.1, and 1.0 mg/mL) was transferred, with five instar nauplii included for each treatment. The plates were then incubated for 24, 48, and 72 h. They were kept under a constant light source and at room temperature. During the exposure to the as-synthesized material, the nauplii were not fed. The plates were examined under a microscope at a 4× magnification after the exposure. When there were no movements during the 10-second observation, the number of dead nauplii was counted as the indicator of mortality. Mortality percentages were used to report the data.

Results and Discussion

Following reflux, reductions in GO and $AgNO_3$ could be clearly seen. An indicator that rGO-Ag nanocomposite had formed was the color change from yellowish to dark brown. According to the structure, size, and aggregation of the AgNPs, the specific absorption peak occurs in the region of 380-450 nm (Figure 1(a)) (Ahamed et al. 2021). The corresponding UV-vis absorption spectra of the GO, AgNPs, and rGO-Ag nanocomposite were recorded. Two different characteristic peaks were observed in the absorbance spectra of the GO assigned to different transitions (Figure 1(b)), which agrees with previous reports on GO (Mahmoud et al. 2022). Two strong

absorption peaks can be seen, the first peak (at 227 nm) claiming to be the conjugated (C=C) π-π* transition and the second peak (at 308 nm) claiming to be the carbonyl (C=O) n- π* transition (Adyani & Soleimani 2019). In contrast, the rGO-Ag nanocomposite exhibited a peak at 263 nm which was associated with the excitation of the π-plasmon graphitic bond (Figure 1(b)). This red shift implies that *C. nutans* leaf extract, when used under reflux conditions, reduced the GO. The rGO-Ag nanocomposite spectrum also showed an absorption peak at 425 nm, which was related to the surface plasmon resonance absorption of AgNPs. Our findings supported those of other studies (Ahmad et al. 2021; Jarmoshti et al. 2019).

The XRD pattern of the synthesized GO shows the strongest diffraction peak at a value of 2Θ= 10.12°, which corresponds to the plane (001) (Figure 1(c)). The peaks with 2Θ=38.10°, 44.33°, 64.48°, 77.28°, and 81.76° are the five different diffraction peaks of green-prepared AgNPs that correspond to the crystal planes (111), (200), (220), (311), and (222) (Figure 1(c)). The planes in the Ag cubic structure were represented by the diffraction peaks in the rGO-Ag nanocomposite XRD pattern at 2Θ values of 38.14°, 44.28°, 64.57°, 77.42°, and 81.40°, which corresponded with the standard card of Ag (JCPDS 04-0783) (Figure 1(c)). The incorporation of GO did not change the original structure of the metallic Ag, as seen by the XRD spectra, which showed that all the peaks of the rGO-Ag nanocomposites resembled those of pure AgNPs and accorded well with observations in the published literature (Al-Marri et al. 2015; Bhangoji et al. 2021). Other peaks were seen, which could have been due to the plant extract's crystalline impurities.

The FTIR spectra of the *C. nutans* leaf extract (PE), GO, Ag, and rGO-Ag nanocomposites ranging between 4000 and 500 cm^{-1} are presented in Table 1. The FTIR graph of the GO (Figure 2(c)) bands shows the oxidation

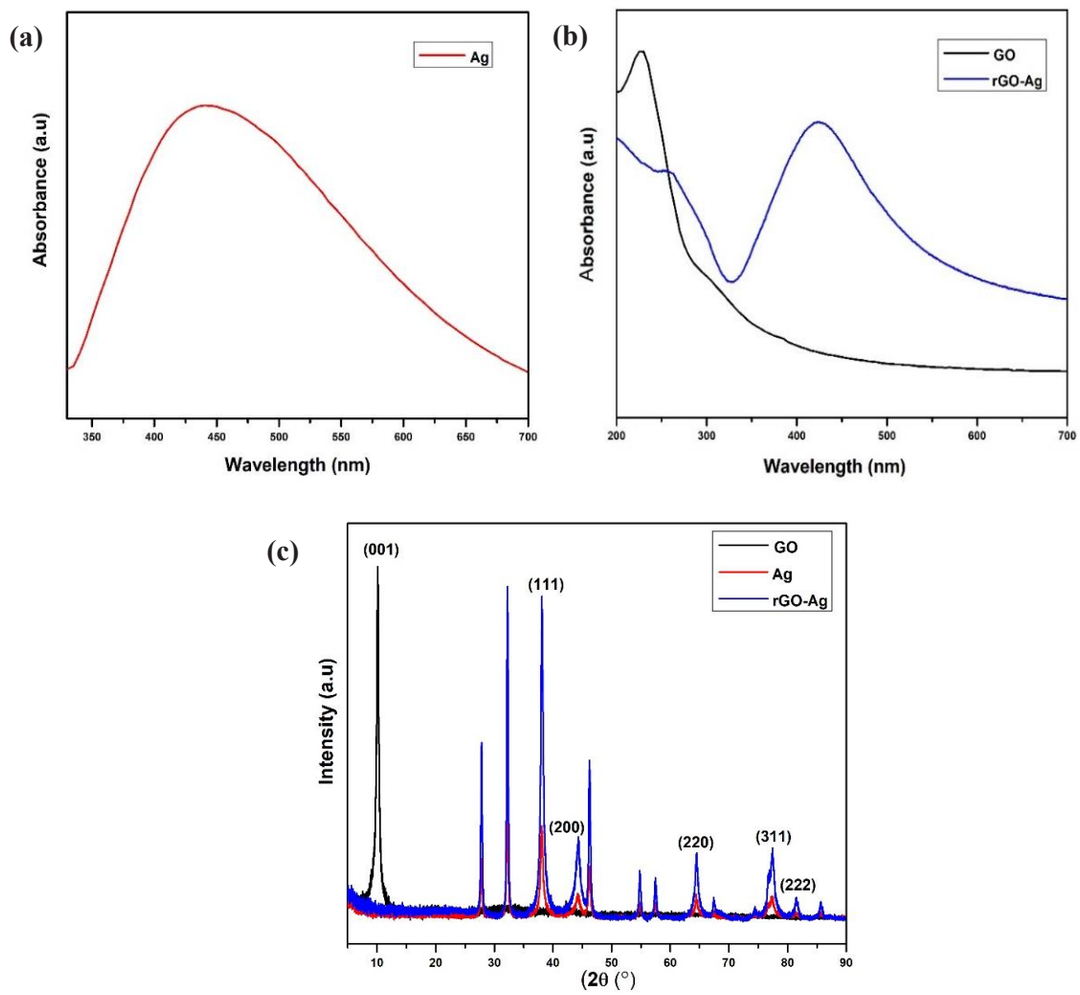

FIGURE 1. UV-Visible spectra of (a) AgNPs, (b) GO and rGO-Ag nanocomposite prepared from *C. nutans* leaf extract and (c) XRD patterns of AgNPs, GO and rGO-Ag nanocomposites

of graphite. The FTIR spectra of the *C. nutans* leaf extracts and AgNPs are shown in Figure 2(d) and Figure 2(b). Based on the FTIR spectra, the *C. nutans* leaf extract peaks show a reduction on the AgNPs spectra. Very similar absorption characteristics were also observed for the rGO-Ag nanocomposite, which denotes that the presence of Ag did not influence the GO (Figure 2(a)). After the reduction process, the FTIR peaks associated with the GO typically either vanish or their intensities reduce significantly, confirming the production of the rGO-Ag nanocomposite.

As shown in Figure 3, the morphology of the GO, AgNPs, and rGO-Ag nanocomposite was examined using FESEM. The average diameter distribution of the AgNPs and rGO-Ag nanocomposites was calculated using Image J software. The FESEM image shows a wrinkly GO sheet (Figure 3(a)). The homogeneous spherical forms of the AgNPs, whose diameters vary from 25 to 80 nm, can be seen in Figure 3(b). The average particle size was roughly 47 ± 15 nm, similar to the findings presented in previously published literature (Ahamed et al. 2021). Through the bioreduction process, the FESEM picture shows the decorated AgNPs on the surface of the crumbled GO sheet with curved edges (shown by the red arrows) (Figure 3(c)). The immobilized AgNPs are spherical in form and range in diameter from 26 to 68 nm. According to the particle size measurements, the average particle size is 48 ± 11 nm. In agreement with our findings, Karthik, Swathi, and Pandi Prabha (2020) found that the co-reduction of Ag ions and GO in the presence of *Brassica nigra* aqueous extract produced rGO-Ag nanocomposites with comparable structural configurations.

TABLE 1. List of functional groups of FTIR spectra of PE, GO and AgNPs

PE	GO	AgNPs	rGO-Ag	Functional groups	Reference
3255	3272	3226	3308	O-H stretching N-H stretching	Basiri, Mehdinia & Jabbari 2018; Noor Hashim et al. 2019; Lim et al. 2022; Siti Nur Aishah et al. 2020
-	-	2906	2928	C-H stretching	
-	-	2347	2355	C=O stretching	
-	1732	-	-	C=O stretching	
1608	1622	1633	1611	C=C stretching N-H bending C=O stretching	
1405	1403	-	-	O-H bending of phenol or tertiary alcohol groups or carboxylic acid groups	
1350	-	1365	-		
-	1229	1216	1209	C-O stretching	
-	1166	-	-	C-O stretching	
1074	1015	1053	1060	C-O stretching of ether or alcohol C-N stretching	

Based on the EDS, the quantitative elemental composition of the GO, AgNPs, and rGO-Ag nanocomposites shows the proportions of each element in the composites, as indicated in Table 2. Carbon (C), oxygen (O), sulfur (S), and chlorine (Cl) were all found to be present in the chemical composition of the GO sheet, with relative weight percentages of 66.8 wt%, 30.3 wt%, 2.0 wt% and 0.9 wt%, respectively. Due to

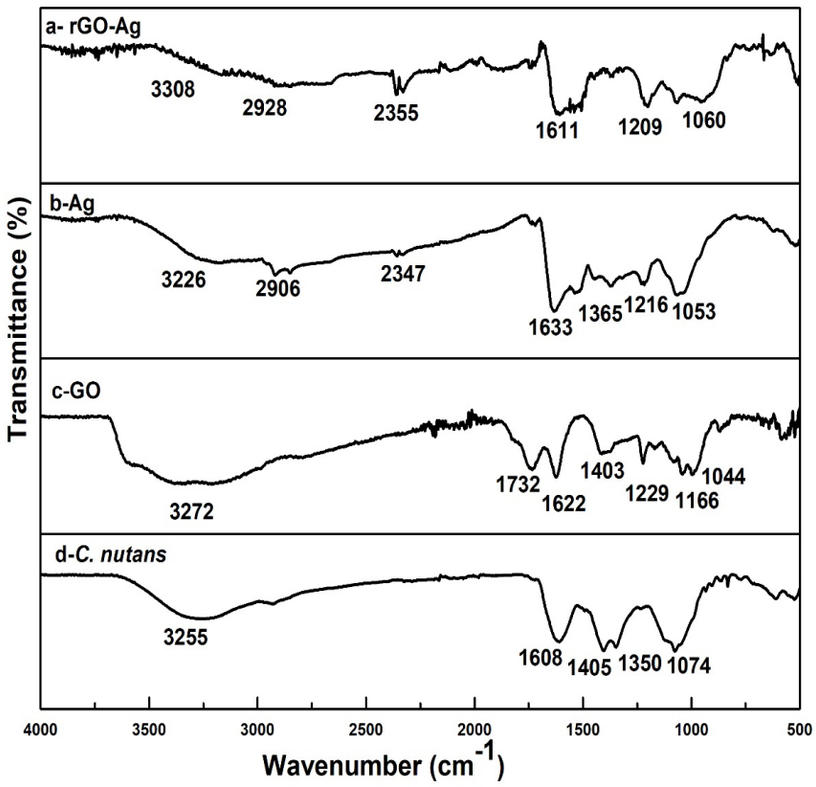

FIGURE 2. FTIR spectra of (a) rGO-Ag nanocomposites, (b) Ag, (c) GO, and (d) *C. nutans* leaf extracts

the use of H_2SO_4 and HCl in the production of GO, S and Cl were present (Karthik, Swathi & Pandi Prabha 2020). The creation of AgNPs is indicated by a strong peak of elemental Ag at about 86.3 wt% in the EDS spectrum. The biomolecules in the *C. nutans* leaf extract, however, may have been the source of the additional peaks connected to the C, O, Cl, and S (Krishnaraj et al. 2022). The presence of AgNPs decorated on the GO sheets surfaces was confirmed by the rGO-Ag nanocomposite EDS spectra, which showed the largest peak was of Ag (84.3%) followed by C (9.1%) (Rodríguez-González et al. 2016).

Using cyclic voltammetry (CV) and 5 mM of $K_3Fe(CN)_6$ containing 0.1 M KCl solution, the electrochemical properties of bare SPCE, GO-SPCE, Ag-SPCE, and rGO-Ag SPCE were investigated. At a scan rate of 100 mV/s, the analysis was conducted in the potential range of -0.3 V to 0.7 V. The electrochemical behavior of the SPCEs before and after treatment with the rGO-Ag nanocomposite is shown in Figure 4. The rGO-Ag nanocomposite electrode increased anodic current about 1.29 times more tthan AgNPs and 1.34 times more than GO. The augmentation of the electron transfers rate of the rGO-Ag SPCE in comparison to the bare-SPCE was attributed to an increase in the peak current. This outcome was consistent with reports from a prior study (Qu et al. 2011). Because of the support provided by the AgNPs on the surface of the GO, the rGO-Ag SPCE displayed excellent sensitivity and facilitated electron transport between the electrolyte solution and the working electrode (Vu et al. 2022).

As shown in Figure 5, the disc diffusion test was used to examine the antibacterial activity of the GO, PE, AgNPs, and rGO-Ag nanocomposites against the microbiological species *E. coli* and *S. aureus*. The results, expressed as a zone of inhibition in mm (Table 3), show that the plate containing GO and PE had no inhibitory zone for the *E. coli* and *S. aureus* microorganisms (Figure 5(a)). This demonstrated that GO has no antibacterial properties that might have a harmful effect in the surrounding area (Khorrami et al. 2019; Ruiz et al. 2011). The benign behavior of the GO

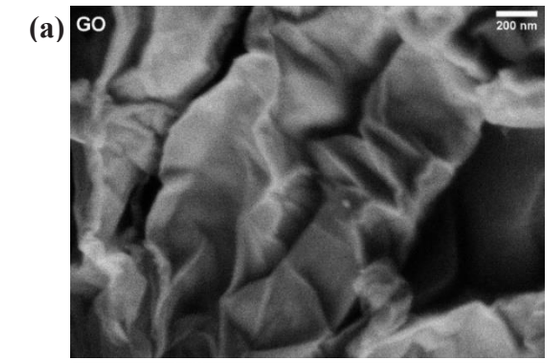

Details	Ag	rGO-Ag
Minimum	25	26
Maximum	80	68
Mean	47	48
Standard deviation	15	11

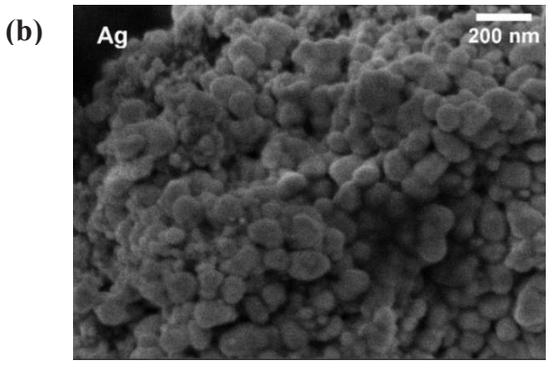

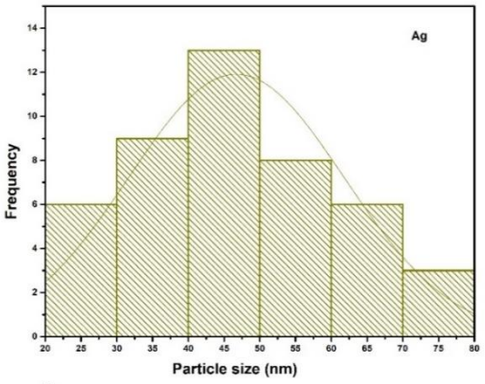

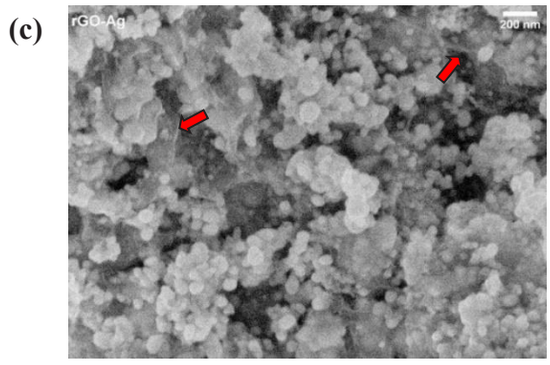

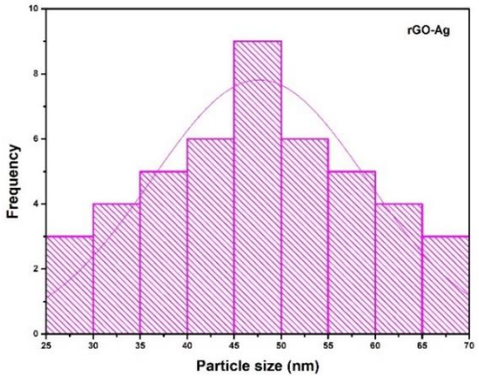

FIGURE 3. FESEM image of the (a) GO and particle size measurement table, (b) AgNPs and particle distribution, and (c) rGO-Ag nanocomposite and particle distribution

was noticed, consistent with earlier studies (Khorrami et al. 2019). In contrast to the *S. aureus* bacteria, which had inhibition zones of 10.92 ± 0.65 mm, as shown in Figure 5(b), AgNPs demonstrated the best antibacterial ability against E. coli bacteria, with inhibition zones of 11.79 ± 0.14 mm. This suggests it displayed slightly stronger antibacterial activity against Gram-negative bacteria. Khane et al. (2022) investigated the antibacterial efficacy of AgNPs against both Gram-positive and Gram-negative bacteria, observing similar findings. The various cell wall structures and antibacterial strategies employed by Ag ions against various bacterial cells may have caused the diverse AgNPs susceptibilities. For instance, Gram-positive bacteria have a peptidoglycan layer that is more resistant to Ag+ transport than the thin peptidoglycan layer of Gram-negative bacteria (Gómez de Saravia et al. 2020). With inhibition zones of 11.86 ± 0.29 mm and 11.99 ± 0.26 mm, respectively, Figure 5(c) demonstrates the outstanding antibacterial activity of the rGO-Ag nanocomposites against both *E. coli* and *S. aureus*

bacteria. Evidently, adding AgNPs to the surface of GO enhanced its antibacterial properties. These results are consistent with previously published findings (Soleymani, Rafigh & Hekmati 2020). The rGO-Ag nanocomposite buildup in the bacterial membrane results in the gradual release of proteins and lipopolysaccharide molecules, which damages the membranes structure and results in the death of the microorganisms (Rajeswari & Amutha 2017). Uncertainty remains regarding the mechanism of the interaction between the component.

TABLE 2. EDS analysis of GO, Ag, and rGO-Ag nanocomposites

Atom	Elemental compound weight percentage (%)					
	Ag	C	O	S	Cl	Si
GO	0.0	66.8	30.3	2.0	0.9	0.0
Ag	86.3	5.4	1.1	0.3	6.9	0.0
rGO-Ag	84.3	9.1	1.4	0.3	4.8	0.1

TABLE 3. Diameter of inhibition zone of GO, PE, Ag, and rGO-Ag nanocomposite using disc diffusion method against Gram-negative and Gram-positive bacteria

Code	Microorganisms	GO	PE	Ag	rGO-Ag
ATCC 25922	*E. coli*	NZ	NZ	11.79 ± 0.14	11.86 ± 0.29
ATCC 43300	*S. aureus*	NZ	NZ	10.92 ± 0.65	11.99 ± 0.26

NZ: no zone inhibition. The data was presented as mean ± standard deviation of three independent experiments

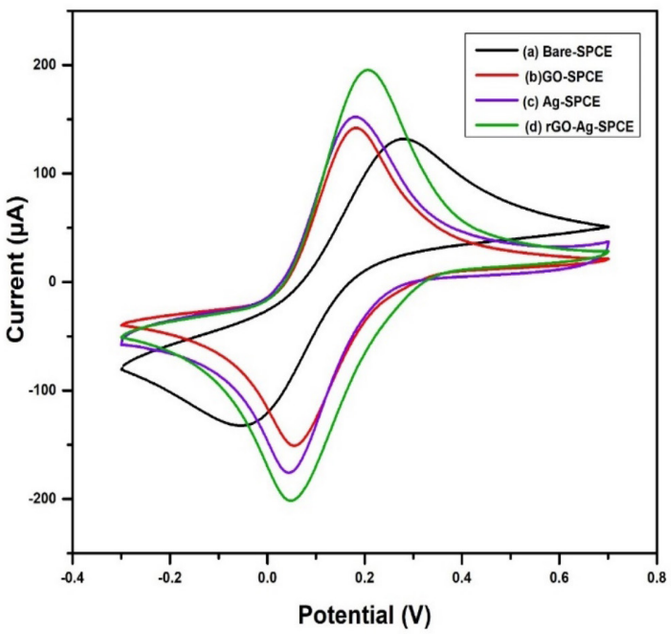

FIGURE 4. Electrochemical properties of bare-SPCE, GO-SPCE, Ag-SPCE, and rGO-Ag-SPCE

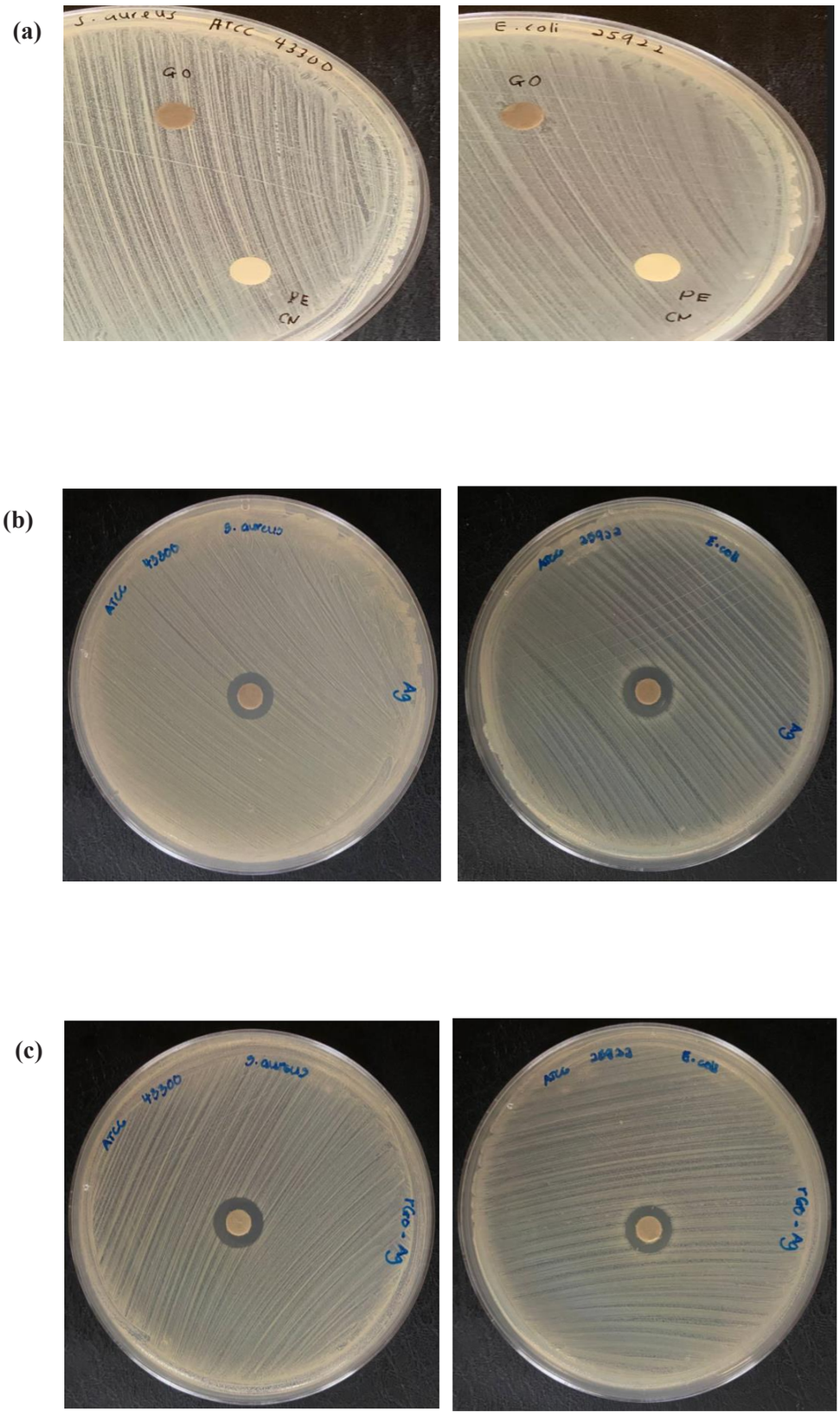

FIGURE 5. Antibacterial activity of (a) GO and plant extract, (b) AgNPs and (c) rGO-Ag nanocomposite (1 mg/mL) against *E. coli* and *S. aureus*

A. salina is a nonselective filter feeder that can consume particles up to 50 µm in size. The primary functions of *A. salina* are ingesting and excreting, making it a relatively simple crustacean in comparison to others. The reduction of nanoparticle aggregates seen under a microscope supports earlier research showing that *A. salina* eats nanoparticles after exposure (Zhu et al. 2017). Larval mortality upon exposure and cyst hatchability are frequently utilized as endpoint criteria, and the sensitivity of both test has been researched (Nunes et al. 2006). From Figure 6(a) and 6(b), it can be deduced that the hatching percentage of the AgNPs and rGO-Ag nanocomposites were dose-dependent. The number of hatched cysts exposed to the nanoparticles reduced in conjunction with the increasing concentration of nanoparticles. About 80% of the cysts in the control hatched in 24 h. The hatching capability of the AgNPs and rGO-Ag nanocomposites exposed to 0.001-0.1 mg/mL within 24 h was slower than that of the control owing to the diffusion of AgNPs via the outer layer of the cyst, in accordance with a previous study (Arulvasu et al. 2014).

On the other hand, more cysts hatched after 48 h when the cysts were exposed to AgNPs and rGO-Ag nanocomposites. Most cysts treated with the AgNPs and rGO-Ag nanocomposites at 0.001 mg/mL had a hatching rate of more than 50%, suggesting biocompatibility at low nanocomposite concentrations. At concentrations of more than 0.01 mg/mL, the number of hatched cysts

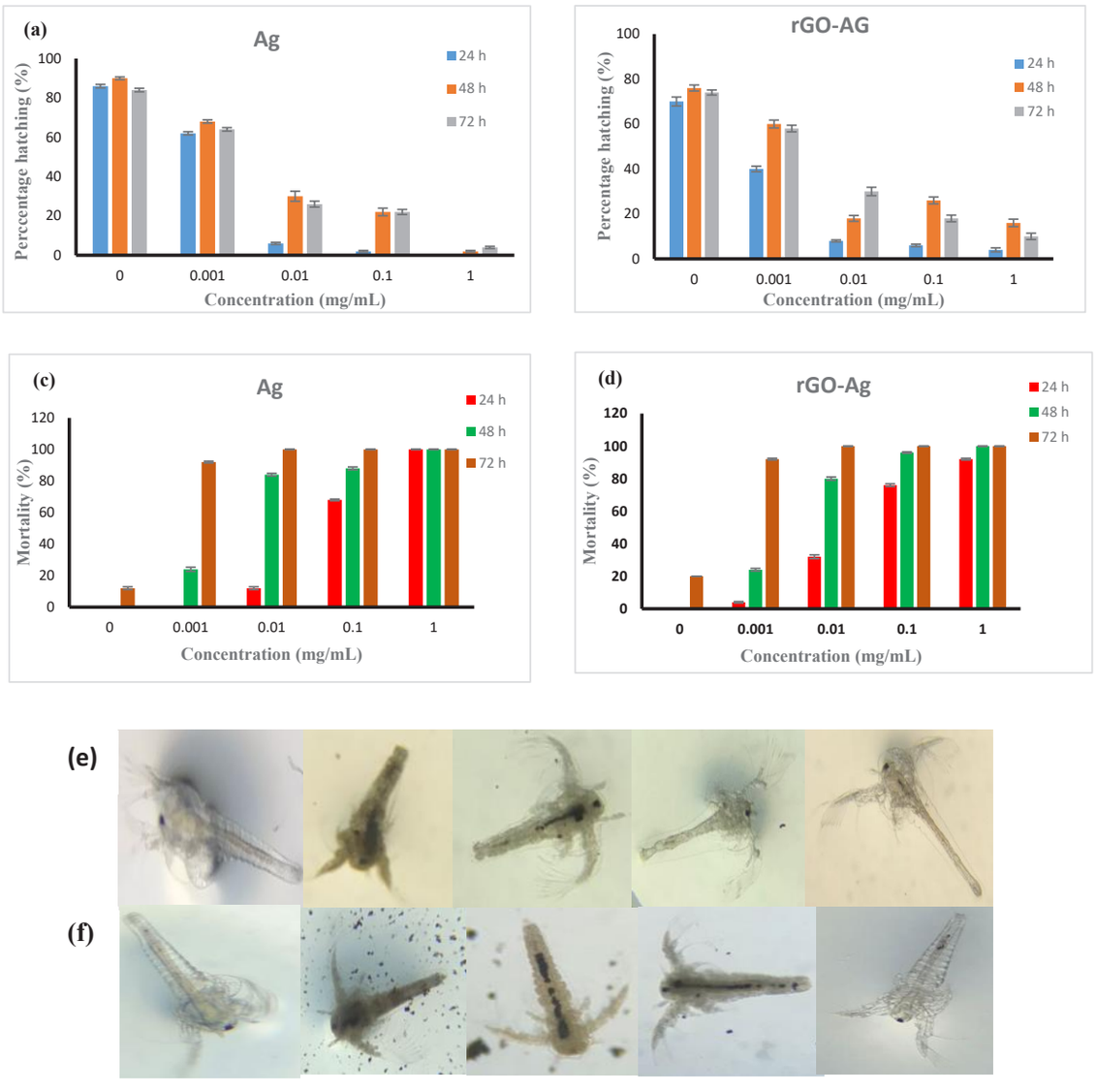

FIGURE 6. Hatching percentage of (a) AgNPs and (b) rGO-Ag nanocomposite. Mortality percentage of (c) AgNPs and (d) rGO-Ag nanocomposite. Image of *A. salina* after 72 h of mortality assay under different concentration (0, 1, 0.1, 0.01, and 0.001 mg/mL) (e) AgNPs and (f) rGO-Ag nanocomposite

was less than 50% for both the AgNPs and rGO-Ag nanocomposites, indicating their non-biocompatibility with *A. salina*. This is in agreement with previous literature suggesting that oxidative stress increased when partially developed cysts were treated with nanoparticles (Rekulapally et al. 2019). Figure 6(c) and 6(d) illustrates the mortality percentage of *A. salina* exposed to AgNPs and rGO-Ag nanocomposites. The *A. salina* consumed the particulate suspended in the salt water, as shown by the black accumulation in the *A. salina* gut in Figures 6(e) and 6(f). The *A. salina* exposed to both AgNPs, and rGO-Ag nanocomposites had a high mortality rate, even at a low dosage of 0.001 mg/mL. Most of the *A. salina* exposed to the nanoparticles at concentrations of 0.01 mg/mL to 1 mg/mL died at 48 h and 72 h, indicating high mortality rates. Previous researchers have stated that this might have been due to gut accumulation of the nanoparticles, which caused the development of reactive oxygen species and superoxide (Rekulapally et al. 2019).

Conclusion

In this study, we synthesized AgNPs and rGO-Ag nanocomposites and characterized them using UV-vis, XRD, FTIR, FESEM and EDS. The FESEM micrographs clearly show the formation of GO sheets decorated with AgNPs 48 nm in size. The electrochemical activity of the rGO-Ag nanocomposite was investigated using CV. According to the findings, the rGO-Ag nanocomposite had greater anodic and cathodic current peaks, making it a potentially useful material for biosensors and other electrochemical applications. *E. coli* and *S. aureus* were successfully combatted by the rGO-Ag nanocomposite. The findings suggest that the rGO-Ag nanocomposite may be a potent antibacterial substance. The study also showed the toxicity effect of AgNPs and rGO-Ag nanocomposites on *A. salina* and evaluated the hatching and mortality percentage. The outcomes of the hatching and mortality tests showed that modest dosages of AgNPs and rGO-Ag nanocomposite were biocompatible with *A. salina*. All application areas gain new perspectives from the use of biological sources in the nanoparticle synthesis process. To increase the practicality of graphene in many sectors, comparative investigations of GO, AgNPs, and rGO-Ag nanocomposites will offer insights into the doping of metal nanoparticles in graphene moieties.

Acknowledgements

The authors express their sincere thanks to Professor Tan Wen Siang from the Faculty of Biotechnology and Biomolecular Sciences, Universiti Putra Malaysia for providing ultraviolet-visible spectroscopy usage. The authors also thankful to Institute of Bioscience, Universiti Putra Malaysia for providing bacterial strains and Institute of Nanoscience and Nanotechnology, Universiti Putra Malaysia for providing instrumental usage. This work was supported by Kurita Water and Environment Foundation, Tokyo, Japan (Grant number: 21Pmy154-31k).

References

Abboud, Z., Vivekanandhan, S., Misra, M. & Mohanty, A.K. 2016. Leaf extract mediated biogenic process for the decoration of graphene with silver nanoparticles. *Materials Letters* 178: 115-119.

Adyani, S.H. & Soleimani, E. 2019. Green synthesis of Ag/Fe_3O_4/RGO nanocomposites by punica granatum peel extract: Catalytic activity for reduction of organic pollutants. *International Journal of Hydrogen Energy* 44: 2711-2730.

Ahamed, M., Akhtar, M.J., Majeed Khan, M.A. & Alhadlaq, H.A. 2021. A novel green preparation of Ag/Rgo Nanocomposites with highly effective anticancer performance. *Polymers* 13: 3350.

Ahmad, M.A., Aslam, S., Mustafa, F. & Arshad, U. 2021. Synergistic antibacterial activity of surfactant free Ag–GO nanocomposites. *Scientific Reports* 11: 1-9.

Ahmad, N., Al-Fatesh, A.S., Wahab, R., Alam, M. & Fakeeha, A.H. 2020. Synthesis of silver nanoparticles decorated on reduced graphene oxide nanosheets and their electrochemical sensing towards hazardous 4-nitrophenol. *Journal of Materials Science: Materials in Electronics* 31(14): 11927-11937.

Al-Marri, A.H., Khan, M., Khan, M., Adil, S.F., Al-Warthan, A., Alkhathlan, H.Z., Tremel, W., Labis, J.P., Siddiqui, M.R.H. & Tahir, M.N. 2015. *Pulicaria glutinosa* extract: A toolbox to synthesize highly reduced graphene oxide-silver nanocomposites. *International Journal of Molecular Sciences* 16(1): 1131-1142.

Allafchian, A., Vahabi, M.R., Hossein Jalali, S.A., Mahdavi, S.S., Sepahvand, S. & Farhang, H.R. 2022. Design of green silver nanoparticles mediated by *Ferula ovina* Boiss. Extract with enhanced antibacterial effect. *Chemical Physics Letters* 791: 139392.

Arulvasu, C., Jennifer, S.M., Prabhu, D. & Chandhirasekar, D. 2014. Toxicity effect of silver nanoparticles in brine shrimp *Artemia*. *The Scientific World Journal* 2014: Article ID. 256919.

Azemi Ahmad Khusairi, Siti Safiah Mokhtar & Aida Hanum Ghulam Rasool. 2020. *Clinacanthus nutans*: Its potential against diabetic vascular diseases. *Brazilian Journal of Pharmaceutical Sciences* 56: e18838.

Bal, M., Tumer, M. & Kose, M. 2022. Synthesis of reduced graphene oxide-based hybrid compounds and investigation of their sensing behavior against some nitroaromatic explosives. *Materials Chemistry and Physics* 289: 126480.

Basiri, S., Mehdinia, A. & Jabbari, A. 2018. Green synthesis of reduced graphene oxide-Ag nanoparticles as a dual-responsive colorimetric platform for detection of dopamine and Cu^{2+}. *Sensors and Actuators, B: Chemical* 262: 499-507.

Bhangoji, J.C., Sahoo, S., Satpati, A.K. & Shendage, S.S. 2021. Facile and green synthesis of silver nanoparticle-reduced graphene oxide composite and its application as nonenzymatic electrochemical sensor for hydrogen peroxide. *Current Chemistry Letters* 10: 295-308.

Chinnaraj, S., Palani, V., Yadav, S., Arumugam, M., Sivakumar, M., Maluventhen, V. & Singh, M. 2021. Green synthesis of silver nanoparticle using *Goniothalamus wightii* on graphene oxide nanocomposite for effective voltammetric determination of metronidazole. *Sensing and Bio-Sensing Research* 32: 100425.

Dinh, D.A., Hui, K.S., Hui, K.N., Cho, Y.R., Zhou, W., Hong, X. & Chun, H.H. 2014. Green synthesis of high conductivity silver nanoparticle-reduced graphene oxide composite films. *Applied Surface Science* 298: 62-67.

Dominic, R.M., Punniyakotti, P., Balan, B. & Angaiah, S. 2022. Green synthesis of reduced graphene oxide using plectranthus amboinicus leaf extract and its supercapacitive performance. *Bulletin of Materials Science* 45: 1-8.

Gómez de Saravia, S.G., Rastelli, S.E., Angulo-Pineda, C., Palza, H. & Viera, M.R. 2020. Anti-adhesion and antibacterial activity of silver nanoparticles and graphene oxide-silver nanoparticle composites. *Revista Materia* 25(2): 1-9.

Handayani, M., Suwaji, B.I., Asih, G.I.N., Kusumaningsih, T., Kusumastuti, Y., Rochmadi & Anshori, I. 2022. *In-situ* synthesis of reduced graphene oxide/silver nanoparticles (RGO/AgNPs) nanocomposites for high loading capacity of acetylsalicylic acid. *Nanocomposites* 8: 74-80.

Herbin, H., Basalius, M., Amalanathan, A.M., Michael Mary, M.S., Maria Lenin, M., Parvathiraja, C., Siddiqui, M.R., Wabaidur, S.M. & Islam, M.A. 2022. Synthesis of silver nanoparticles using *Syzygium malaccense* fruit extract and evaluation of their catalytic activity and antibacterial properties. *Journal of Inorganic and Organometallic Polymers and Materials* 32: 1103-1115.

Jarmoshti, J.A., Nikfarjam, A., Hajghassem, H. & Banihashemian, S.M. 2019. Visible light enhancement of ammonia detection using silver nanoparticles decorated on reduced graphene oxide. *Materials Science & Engineering B* 6: 066306.

Karthik, C., Swathi, N., Pandi Prabha, S. & Caroline, D.G. 2020. Green synthesized RGO-AgNP hybrid nanocomposite - An effective antibacterial adsorbent for photocatalytic removal of DB-14 dye from aqueous solution. *Journal of Environmental Chemical Engineering* 8(1): 103577.

Khane, Y., Benouis, K., Albukhaty, S., Sulaiman, G.M., Abomughaid, M.M., Al Ali, A., Aouf, D., Fenniche, F., Khane, S., Chaibi, W., Henni, A., Bouras, H.D. & Dizge, N. 2022. Green synthesis of silver nanoparticles using aqueous citrus limon zest extract: Characterization and evaluation of their antioxidant and antimicrobial properties. *Nanomaterials* 12(12): 2013.

Khorrami, S., Abdollahi, Z., Eshaghi, G., Khosravi, A., Bidram, E. & Zarrabi, A. 2019. An improved method for fabrication of Ag-GO nanocomposite with controlled anti-cancer and anti-bacterial behavior: A comparative study. *Scientific Reports* 9: 1-10.

Krishnaraj, C., Krishnamoorthi Kaliannagounder, V., Rajan, R., Ramesh, T., Kim, C.S., Park, C.H., Liu, B. & Yun, S.I. 2022. Silver nanoparticles decorated reduced graphene oxide: Eco-friendly synthesis, characterization, biological activities and embryo toxicity studies. *Environmental Research* 210: 112864.

Lim, V., Chong, H.W., Nozlena Abdul Samad, Siti Aisyah Abd Ghafar, Ida Shazrina Ismail, Rafeezul Mohamed, Yong, Y.K., Gan, C.Y. & Tan, J.J. 2022. Vibrational spectroscopy-based chemometrics analysis of *Clinacanthus nutans* extracts after postharvest processing and extract effects on cardiac C-Kit cells. *Evidence-Based Complementary and Alternative Medicine* 2022: 1967593.

Mahendran, N., Anand, B., Rajarajan, M., Muthuvel, A. & Mohana, V. 2021. Green synthesis, characterization and antimicrobial activities of silver nanoparticles using *Cissus quadarangularis* leaf extract. *Materials Today: Proceedings* 49: 2620-2623.

Mahmoud, A.E.D., Hosny, M., El-Maghrabi, N. & Fawzy, M. 2022. Facile synthesis of reduced graphene oxide by *Tecoma stans* extracts for efficient removal of Ni (II) from water: Batch experiments and response surface methodology. *Sustainable Environment Research* 32: 1-16.

Marcano, D.C., Kosynkin, D.V., Berlin, J.M., Sinitskii, A., Sun, Z., Slesarev, A., Alemany, L.B., Lu, W. & Tour, J.M. 2010. Improved synthesis of graphene oxide. *ACS Nano* 4(8): 4806-4814.

Mindivan, F. & Göktaş, M. 2020. Rosehip-extract-assisted green synthesis and characterization of reduced graphene oxide. *ChemistrySelect* 5(29): 8980-8985.

Minh, P.N., Hoang, V.T., Dinh, N.X., Hoang, O.V., Cuong, N.V., Hop, D.T.B., Tuan, T.Q., Khi, N.T., Huy, T.Q. & Le, A.T. 2020. Reduced graphene oxide-wrapped silver nanoparticles for applications in ultrasensitive colorimetric detection of Cr(vi) ions and the carbaryl pesticide. *New Journal of Chemistry* 44(18): 7611-7620.

Noor Hashim, Noor Haslinda, Amatul Hamizah Ali, Alfi Khatib & Jalifah Latip. 2019. Discrimination of *Clinacanthus nutans* extracts and correlation with antiplasmodial activity using ATR-FTIR fingerprinting. *Vibrational Spectroscopy* 104: 102966.

Nunes, B.S., Carvalho, F.D., Guilhermino, L.M. & Van Stappen, G. 2006. Use of the genus artemia in ecotoxicity testing. *Environmental Pollution* 144: 453-462.

Olorunkosebi, A.A., Eleruja, M.A., Adedeji, A.V., Olofinjana, B., Fasakin, O., Omotoso, E., Oyedotun, K.O., Ajayi, E.O.B. & Manyala, N. 2021. Optimization of graphene oxide through various hummers' methods and comparative reduction using green approach. *Diamond and Related Materials* 117: 108456.

Ooi Swee Hong, Nur Mazidah Noor Mohamed, Ravi Kumar Kalaichelvam, Vuanghao Lim, & Ida Shazrina Ismail. 2021. Effects of *Clinacanthus nutans* extracts on cytokine secretion in PMA-induced U937 macrophage cells. *Research Journal of Pharmacognosy* 8: 27-35.

Parthipan, P., Cheng, L., Rajasekar, A., Govarthanan, M. & Subramania, A. 2021. Biologically reduced graphene oxide as a green and easily available photocatalyst for degradation of organic dyes. *Environmental Research* 196: 110983.

Pumera, M. 2010. Graphene-based nanomaterials and their electrochemistry. *Chemical Society Reviews* 39: 4146-4157.

Qu, F., Lu, H., Yang, M. & Deng, C. 2011. Electrochemical immunosensor based on electron transfer mediated by graphene oxide initiated silver enhancement. *Biosensors and Bioelectronics* 26: 4810-4814.

Rai, S., Bhujel, R., Biswas, J. & Swain, B.P. 2021. Biocompatible synthesis of RGO from ginger extract as a green reducing agent and its supercapacitor application. *Bulletin of Materials Science* 44: 1-11.

Rajeswari, R., Gurumallesh Prabu, H. & Amutha, M. 2017. One pot hydrothermal synthesis characterizations of silver nanoparticles on reduced graphene oxide for its enhanced antibacterial and antioxidant properties. *IOSR Journal of Applied Chemistry* 10: 64-69.

Rekulapally, R., Murthy Chavali, L.N., Idris, M.M. & Singh, S. 2019. Toxicity of TiO_2, SiO_2, ZnO, CuO, Au and Ag engineered nanoparticles on hatching and early Nauplii of *Artemia* sp. *PeerJ* 6: e6138.

Rodríguez-González, C., Velázquez-Villalba, P., Salas, P. & Castaño, V.M. 2016. Green synthesis of nanosilver-decorated graphene oxide sheets. *IET Nanobiotechnology* 10: 301-307.

Rudrappa, M., Rudayni, H.A., Assiri, R.A., Bepari, A., Basavarajappa, D.S., Nagaraja, S.K., Chakraborty, B., Swamy, P.S., Agadi, S.N., Niazi, S.K. & Nayaka, S. 2022. *Plumeria alba*-Mediated green synthesis of silver nanoparticles exhibits antimicrobial effect and anti-oncogenic activity against glioblastoma U118 MG cancer cell line. *Nanomaterials (Basel)* 12(3): 493.

Ruiz, O.N., Shiral Fernando, K.A., Wang, B., Brown, N.A., Luo, P.G., McNamara, N.D., Vangsness, M., Sun, Y.P. & Bunker, C.E. 2011. Graphene oxide: A nonspecific enhancer of cellular growth. *ACS Nano* 5: 8100-8107.

Siti Nur Aishah Mat Yusuf, Che Nurul Azieyan Che Mood, Nor Hazwani Ahmad, Doblin Sandai, Chee Keong Lee & Vuanghao Lim. 2020. Optimization of biogenic synthesis of silver nanoparticles from flavonoid-rich *Clinacanthus nutans* leaf and stem aqueous extracts: Biogenic synthesis of *C. nutans* AgNPs. *Royal Society Open Science* 7: 200065.

Soleymani, A.R., Rafigh, S.M. & Hekmati, M. 2020. Green synthesis of RGO/Ag: As evidence for the production of uniform mono-dispersed nanospheres using microfluidization. *Applied Surface Science* 518: 146264.

Tran, H.V., Nguyen, N.D., Tran, C.T.Q., Tran, L.T., Le, T.D., Tran, H.T.T., Piro, B., Huynh, C.D., Nguyen, T.N., Nguyen, N.T.T., Dang, H.T.M., Nguyen, H.L., Tran, L.D. & Phan, N.T. 2020. Silver nanoparticles-decorated reduced graphene oxide: A novel peroxidase-like activity nanomaterial for development of a colorimetric glucose biosensor. *Arabian Journal of Chemistry* 13(7): 6084-6091.

Vu, Q.K., Nguyen, T.H., Le, A.T., Vu, N.P., Ngo, X.D., Nguyen, T.K., Nguyen, T.T., Pham, C.V., Nguyen, T.L., Dang, T.L.T., Tonezzer, M. & Tran, Q.H. 2022. Enhancing electron transfer and stability of screen-printed carbon electrodes modified with AgNP-reduced graphene oxide nanocomposite. *Journal of Electronic Materials* 51: 1004-1012.

Yang, J., Xia, X., He, K., Zhang, M., Qin, S., Luo, M. & Wu, L. 2021. Green synthesis of reduced graphene oxide (RGO) using the plant extract of *Salvia spinosa* and evaluation of photothermal effect on pancreatic cancer cells. *Journal of Molecular Structure* 1245: 131064.

Yu, F., Ma, J., Qi, Y., Song, H., Tan, G., Huang, F. & Yang, M. 2022. Geographical traceability of *Clinacanthus Nutans* with near-infrared pectroscopy and chemometrics. *American Journal of Analytical Chemistry* 13: 63-77.

Zhu, S., Luo, F., Chen, W., Zhu, B. & Wang, G. 2017. Toxicity evaluation of graphene oxide on cysts and three larval stages of *Artemia salina*. *Science of the Total Environment* 595: 101-109.

*Corresponding author; email: azurahanim@upm.edu.my